Supplement of Geosci. Model Dev., 15, 3969–4026, 2022
https://doi.org/10.5194/gmd-15-3969-2022-supplement

Geoscientific Model Development
Open Access
EGU

Supplement of

Description and evaluation of the community aerosol dynamics model MAFOR v2.0

Matthias Karl et al.

Correspondence to: Matthias Karl (matthias.karl@hereon.de)

S1. Description of numerical scenarios

The performance of MAFOR v2.0 was evaluated in three different numerical scenarios that were derived from the literature. The first test (Case 1) concerns the sectional representation of the aerosol size distribution in a scenario of new particle formation in urban areas. The second test (Case 2) investigates the process of coagulation in a chamber experiment under the condition of continuous injection of nanoparticles. The third test (Case 3) concerns the dynamic treatment of semi-volatile inorganic gases by condensation and dissolution. The size distributions of the initial aerosol in Case 1 and 3 and of the emitted particles in Case 2 are given in Table S1.

Table S1: Size distributions of the initial aerosol (Case 1 and 3) and of the emitted particles (Case 2) in the numerical scenarios.

Case	Mode	*N* or *Q*	*GMD* (number) [nm]	σ_A [-]	Diameter range [μm]	Number of size bins
1	Nuc	3810 cm^{-3}	25	1.65	0.0015−2.0	16, 32, 60, 80, 120, 160
	Ait	2320 cm^{-3}	56	2.1		
	Acc	220 cm^{-3}	290	2.0		
2	Nuc	$2x10^9$ m^{-3} s^{-1}	15	1.3	0.001−10.0	80
3	Ait	$1.83x10^5$ cm^{-3}	30	2.2	0.001−10.0	60
	Acc	2900 cm^{-3}	180	2.1		
	Coa	0.6 cm^{-3}	1700	2.0		

S2. Case 1: performance of the sectional representation

In Case 1 it was investigated how the numerical representation of the particle size distribution in the model affects the simulation results, addressing the problem of numerical diffusion during condensation of vapours by varying the number of size bins.

The test focuses on the formation and growth of new particles in urban environments in 10-h test simulations, considering the change of the initial size distribution through nucleation of sulphuric acid-water (using the parameterization of Määttänen et al., 2018a), multicomponent condensation/evaporation, coagulation due to Brownian motion, and dry deposition. The model was run as box model coupled with gas-phase chemistry integration under clear sky conditions. The organic fraction of the pre-existing particles was described with a low volatile organic vapour (with $C^0 = 0.028$ μg m^{-3}). The gas-phase concentrations of the organic vapour and of sulphuric acid followed a semisinusoidal pattern, peaking 4 h after the beginning of the simulation at 1×10^7 cm^{-3} and 5×10^7 cm^{-3}, respectively. The pre-existing particle population corresponded to an urban background particle distribution measured in Helsinki (Finland) during the SAPPHIRE campaign (Hussein et al., 2007; Case I in table 1 and figure 3 therein), with a total PN concentration of 6350 cm^{-3}, typical for summertime (see Table S1). The chemical composition of the size-fractionated particles in the urban background was taken from the LIPIKA study in Helsinki (Pohjola et al., 2007). Model results obtained with 160 size bins were used as a reference, corresponding to a level of resolution that usually reproduces the results of the discrete solution with very good accuracy (Korhonen et al., 2003). Test simulations were carried out using different number of size bins (16, 32, 60, 80, 120, and 160), comparing the final modelled size distributions to the reference solution (160 size bins). The condensation sink was on the order of 3×10^{-2} s^{-1}, about one order of magnitude higher than the coagulation sink.

The evolution of the particle size distribution from the reference model (160 bins) in Fig. S1a shows that the onset of binary nucleation, which requires sufficiently high sulphuric acid concentration, occurred approximately two hours after simulation start. Maximum nucleation rate (0.95 cm^{-3} s^{-1}) coincided with peak H_2SO_4 concentration. Under the given conditions (T = 288 K and RH = 90 %), the nucleation model of Määttänen et al. (2018a) predicts only ion-induced nucleation, while the formation rate from neutral nucleation was zero. The formation of new particles leads to a distinct nucleation mode with a gap between nucleation mode and the growing Aitken mode at about 9−14 nm in diameter. In this size range, the freshly nucleated particles collide rapidly with the Aitken mode particles of the pre-existing particle population and the forming new particles become part of the growing Aitken mode. Fig. S1b displays the final particle size distribution after 10 h for Case 1. The growth by condensation and the coagulation with smaller particles shifted the peak diameter of the Aitken mode from 22 nm in the initial particle distribution to 39 nm in the final particle distribution. The fixed sectional method with 120 bins agrees very well with the reference solution, captures the growth of the nucleation mode accurately, and results in a final size distribution that is almost identical with the reference. Even with 60 bins, the performance is still very good in comparison to the reference, although slight spreading of the nucleation mode due to numerical diffusion can be noted. For lower size resolution, the discretization errors are more relevant, leading to a broader nucleation mode with peak diameter at smaller size. The lowest resolution in the test with 16 bins starts with a much coarser representation of the initial particle distribution. The formation and growth of nucleation mode particles are still reproduced, but the Aitken mode peak is flattened out, so that Aitken mode and Accumulation mode cannot be distinguished. This leads to an increase of the condensation sink and lowers the H_2SO_4 concentration available for new particle formation.

a)

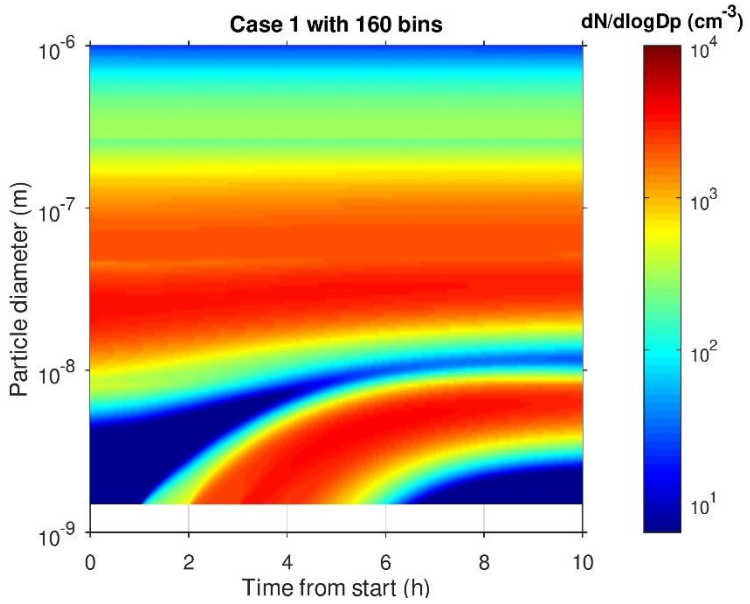

b)

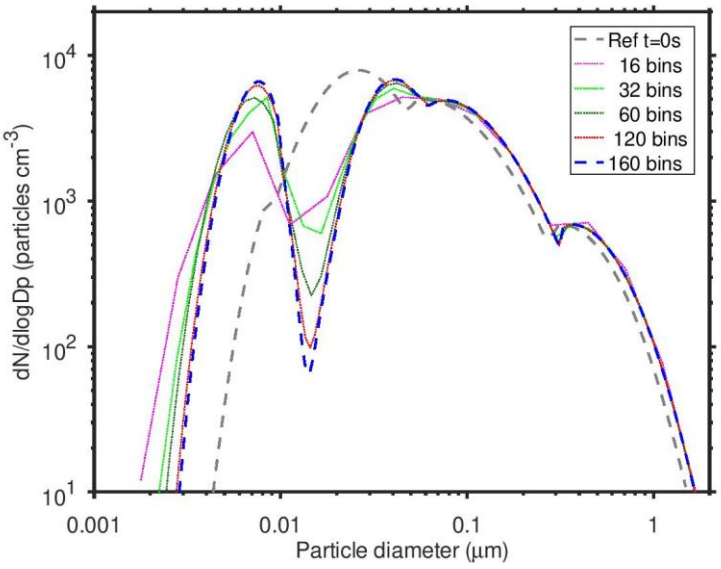

Figure S1. Results from Case 1: a) sequential time evolution of the number size distribution of the reference solution; b) final particle size distribution for different number of size sections, together with the initial size distribution shown as grey dashed line. Particle number concentration on the vertical axis in part (a) and on the contours in part (b) is plotted as $dN/d(log_{10})D_p$.

Quantitative deviations of the final total number concentration, N_{tot}, from the reference are small, even for the low size resolutions, see Table S2. The final N_{tot} in the simulations with 16 bins and 32 bins has an error of 10.2 % and 3.2 %, respectively, which is still acceptable when compared to typical measurement errors for total PN concentration. For size resolutions with 60 bins and higher, the error is less than 1%. The computational time increases exponentially with increasing size resolution. The reference computation takes 50 % more CPU time than the computation with the lowest size resolution in the test.

Table S2: Final particle number concentration and computational time in Case 1 for different number of size bins. The error of final N_{tot} is defined as the relative deviation from the final N_{tot} of the reference run. All calculations were done on a Linux computer (Intel® Core i5-9500TE CPU at 2.20 GHz x6, 7.6 GB RAM). CPU time refers to the full model run.

Number of bins	Final N_{tot} [cm^{-3}]	Error final N_{tot} [%]	CPU time [s]
16	5682	10.2	19.08
32	6126	3.2	19.52
60	6195	2.1	20.94
80	6242	1.4	21.84
120	6297	0.5	25.35
160	6330	0.0	29.85

S3. Case 2: performance of the numerical solution for coagulation

In Case 2, the performance of the model's coagulation process is analysed in the simulation of a chamber experiment in the presence of a continuous emission of nanoparticles. The chamber experiments carried out in Seipenbusch et al. (2008) and the subsequent theoretical analysis (Anand et al., 2012) showed that the evolution of a continuously injected monodisperse aerosol in a closed system exhibits some important features such as peaking behaviour of total number concentration, the formation of a bimodal size distribution, the removal of particles by coagulation and ventilation, as well as the effects of fractal structure of particles. In particular, the development of a distinct secondary mode of larger particles can be explored in this scenario. Anand et al. (2012) have simulated the experiment using a numerical aerosol dynamics model that represents the size distribution by the nodal method, which is a modification of the sectional method, where finite-sized sections are reduced to discrete points, called "nodes", on the size domain (Prakash et al., 2003).

The parameterization of the continuous particle emission source in Case 2 was done in a similar manner as in Anand et al. (2012). Anand et al. (2012) tested two different particle size distributions for the nanoparticle emissions, having count median diameter of 15 and 30 nm, respectively. The aerosol generator used in the experiments by Seipenbusch et al. (2008) produced nanoparticles with approximately log-normal size distributions, centred at 7−8 nm median diameter and $\sigma_A \approx 1.3$. The formation of fractal aggregates and immediate particle growth by self-coagulation may take place at an early stage near the aerosol source, before the actual measurements could take place. First size distribution measurements in the chamber showed a single peak at 15 nm in the initially particle-free chamber (Seipenbusch et al., 2008). It was therefore decided to use a median diameter of 15 nm in the simulation of the experiment.

Case 2 test simulations were performed for 9 hours at T = 298 K, with zero background particles, and a continuous source of 2×10^9 m^{-3} s^{-1} of particles with GMD = 15 nm, having the density of Platinum (Pt), 21450 kg m^{-3}. The aerosol chamber has a volume of 2 m^3 (dimensions $1 \times 1 \times 2$ m). The simulations with MAFOR considered coagulation using the Brownian kernel extended for fractal geometry as the only dynamical process. Removal of particles by ventilation was zero and particle loss to chamber wall surfaces were neglected. Tests were done with fractal dimensions D_f = 3.0 (spherical shape) and D_f = 1.75 to study the effect of fractal geometry. The size of the primary spherules in the fractal agglomerates was assumed to be 5 nm. The size distribution of emitted particles in MAFOR is initialized through the mass distribution in four aerosol modes; and the nanoparticle emissions were placed in the Aitken mode size range. It was not possible to insert particle emissions below the lower Aitken mode diameter limit of ca. 10 nm, which reduced the number of small particles, while the total number of emitted particles was not affected. The performance of the implemented method for coagulation was evaluated by qualitative and quantitative comparison with the numerical results that were obtained with a nodal aerosol dynamics model, published by Anand et al. (2012).

The modelled evolution of the particle size spectra in Case 2 for coagulation with compact spherical particles (D_f = 3.0) in Fig. S3a shows that the size distribution remained unimodal until 1−2 h after simulation start, whereas the secondary peak gradually appeared approx. 5 h after simulation start. While the first peak remained nearly stationary at the size of the emitted nanoparticles, the secondary peak gradually moved to larger sizes. The peak height of the primary mode in terms of $dN/d(lnD_p)$ was at 3.0×10^6 cm^{-3} after 0.5 h and the peak height of the secondary mode was at 2.0×10^5 cm^{-3} after 9 h (600 min); both in good agreement with the modelled particle size distribution for the same case in Anand et al. (2012; figure 6 therein).

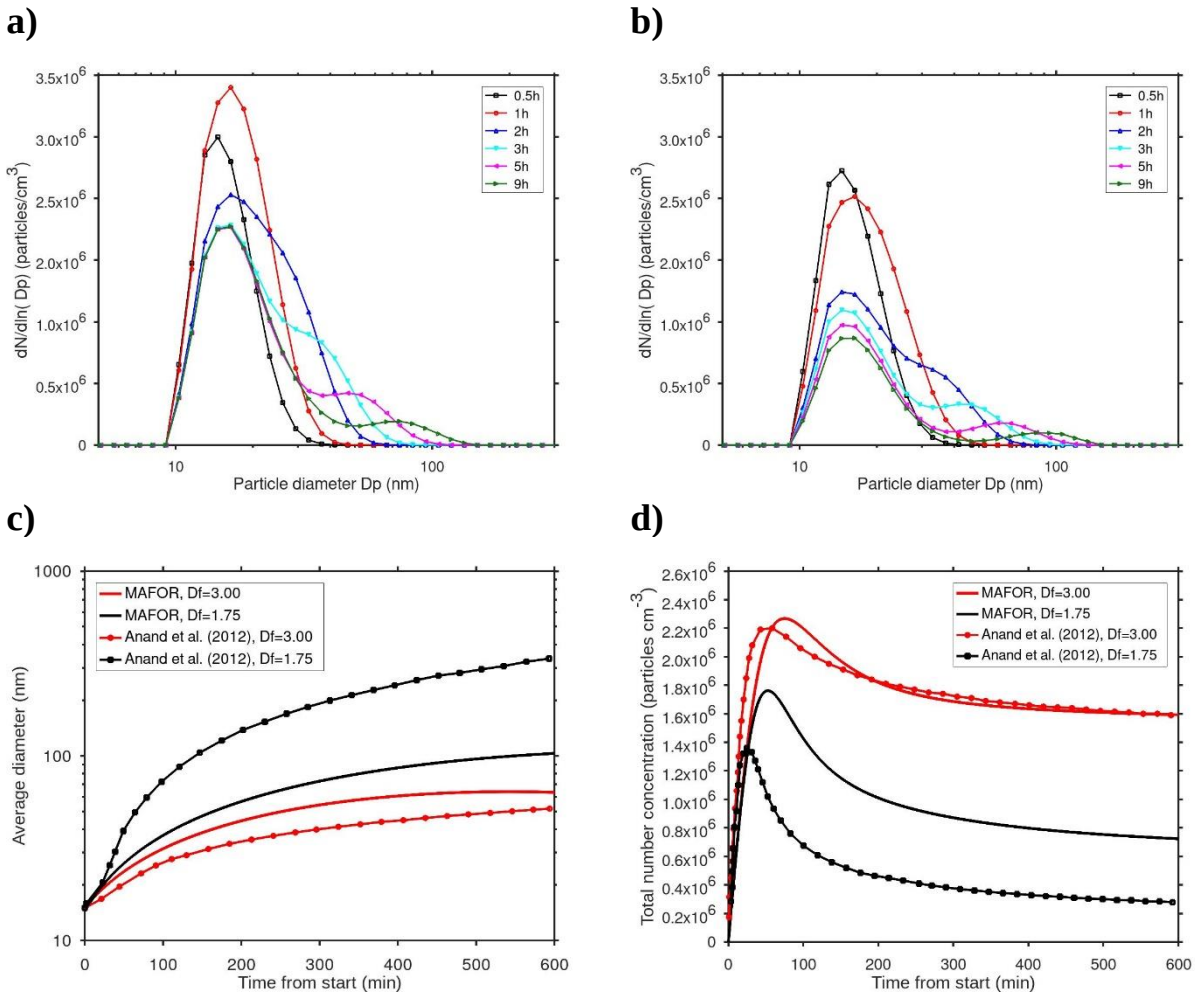

Figure S3. Results from Case 2: a) number size distribution evolution for D_f = 3.0; b) number size distribution evolution for D_f = 1.75; c) average diameter of the particle distribution as function of time and d) total particle number concentrations as function of time. Simulation of particle emissions with GMD = 15 nm, $Q = 2 \times 10^9$ m^{-3} s^{-1}, zero background particles, zero ventilation and no particle losses to chamber surfaces

The effect of fractal geometry on coagulation was tested by considering emitted nanoparticles with fractal shape (D_f = 1.75). The particle size spectra in Fig. S3b shows that the secondary mode forms earlier when fractal particles are considered (ca. 3 h after start). As expected from a discrete-sectional size distribution, the secondary mode flattens when moving to larger diameters. The secondary mode shifts more rapidly to larger sizes for fractal particle than for compact particles. Anand et al. (2012) noted that for fractal particles, the primary peak decreases continuously with time, while for compact particles, the height of the first peak remains almost unchanged. This feature is also found in simulations with MAFOR when comparing the primary peak in Figures S3a and S3b.

Compared to the case with fractal particles in Anand et al. (2012; figure 7 therein), the secondary peak of the fractal size distribution simulated with MAFOR reaches much lower mean particle diameter. The modelled peak diameter of the secondary mode for fractal particles in Anand et al. was ~200 nm after 200 minutes, larger than suggested by the experimental data on particle diameter (Seipenbusch et al., 2008; figure 4 therein) at 200 min experiment time (ca. 110 nm). However, MAFOR substantially underestimates the experimentally observed peak diameter of the secondary mode at 200 min. At the end of the model simulation with MAFOR, the average diameter of the (bimodal) particle size distribution for the fractal particles was slightly larger (103 nm) than for the compact particles (64 nm), see Fig. S3c.

The final average diameter of the modelled fractal particles in the study of Anand et al. (2012) was about three times larger (ca. 340 nm) than in this study (Fig. S3c). For Case 2 with compact particles, modelled total number concentration (Fig. S3d) is in good agreement with the results of Anand et al. (2012). Again, differences are seen for the simulation of fractal particles, for which modelled final N_{tot} was 31 % higher compared to the model results of Anand et al. (2012).

The first reason for faster growth of fractal particles in the nodal aerosol dynamics model used in Anand et al. (2012) compared to the simulation with MAFOR probably lies in the details of the implementation of the fractal geometry, although the same particle morphology was used in both models. A second reason might be the different discretization of the particle size distribution between the sectional and the nodal model, leading to different accuracy of the computed mean particle diameter. However, such differences are considered to be small for the case of pure coagulation (Prakash et al., 2003). The accuracy of the coagulation solution in MAFOR with respect to particle mass conservation is sufficiently high, with an error of less than 0.5 %.

S4. Case 3: performance of the coupled PNG-MOSAIC scheme

In Case 3, the performance of the coupled PNG-MOSAIC scheme is investigated to detect possible oscillatory behaviour in the numerical solution. Simulation of the secondary formation of particles by dissolution/dissociation of HNO_3, condensation of H_2SO_4 and equilibration of NH_3 were performed, using the PNG scheme coupled with MOSAIC solver (Zaveri et al., 2008). The initial conditions for Case 3 were adopted from the tests of the PNG-EQUISOLV II scheme presented in Jacobson (2005a). Aerosol particles were initialized with 10 μg m^{-3} NaCl and 20 μg m^{-3} inert material. The initial gas-phase concentrations were 30 μg m^{-3} HNO_3, 10 μg m^{-3} NH_3, 0.0 μg m^{-3} HCl, and 10 μg m^{-3} H_2SO_4. Several tests were made to examine how the coupled PNG-MOSAIC scheme performs under different concentrations of HNO_3 and NH_3: a) "High-N" using the aforementioned concentrations, b) "Low-NO3" with the same initial conditions except the HNO_3 concentration was 0.1 μg m^{-3} instead of 30 μg m^{-3}, and c) "Low-NH4" using the same initial conditions except the NH_3 concentration was 0.1 μg m^{-3} instead of 10 μg m^{-3}. The atmospheric simulations were done for 12 hours at T = 298 K and RH = 90 %.

Summed mass concentrations of the inorganic aerosol components were compared to results from equilibrium simulations with EQUISOLV II, adopted from Jacobson (2005a). The EQUISOLV II simulations considered only gas-aerosol equilibrium; sulphuric acid was allowed to condense in a non-equilibrium manner, but all other gases were equilibrated with the size distribution during and after condensation. The equilibrium-only solution is used here for reference purposes. Details on the equilibrium-only solution are given in Jacobson (2005a).

During the simulation of Case 3 with different concentrations of N-containing species, H_2SO_4 condensed, HCl and HNO_3 dissolved/dissociated and NH_3 equilibrated with dissolved and dissociated species. The uptake of water occurred at each model time step based on equilibrium

thermodynamics (Binkowski and Shankar, 1995). The calculated water content is handed over to the MOSAIC solver during the operator-split equilibrium calculation for the acids and bases. The operator-split time interval between growth and equilibrium was 115 s in all test simulations. Fig. S2 a-c shows time series of the aerosol mass concentrations, summed over all size bins. Fig. S2 d-f shows the final mass size distributions of aerosol components between 0.01and 10 μm diameter after 12 h simulation time.

In simulation "High-N", with high NH_4 and HNO_3 concentrations (30 μg m^{-3} HNO_3, 10 μg m^{-3} NH_3), an equilibrium was reached within about 6 h, however, in the second half of the simulation nitrate began to form on the coarse mode particles connected to the depletion of chlorine. Available NH_4^+ balances the sulphuric acid in the fine mode aerosol, while the larger particles were not neutralized. The time-dependent summed concentrations of inorganic aerosol species matched the equilibrium levels from EQUISOLV II fairly well.

In simulation "Low-NO3" the performance of PNG-MOSAIC was examined under low nitrate conditions (0.1 μg m^{-3} HNO_3). The scheme with operator-split time interval of 115 s was demonstrated to be very accurate under low nitrate conditions. The summed mass concentration of inorganic species and aerosol water were perfectly aligned with the EQUISOLV II equilibrium-only solution.

The simulation "Low-NH4" examined how the PNG-MOSAIC scheme performs under extremely low ammonia conditions (0.1 μg m^{-3} NH_3). This is a critical test, since the PNG-MOISAIC scheme is based on the assumption that ammonia equilibrates with all particle sizes following the growth of acidic gases.

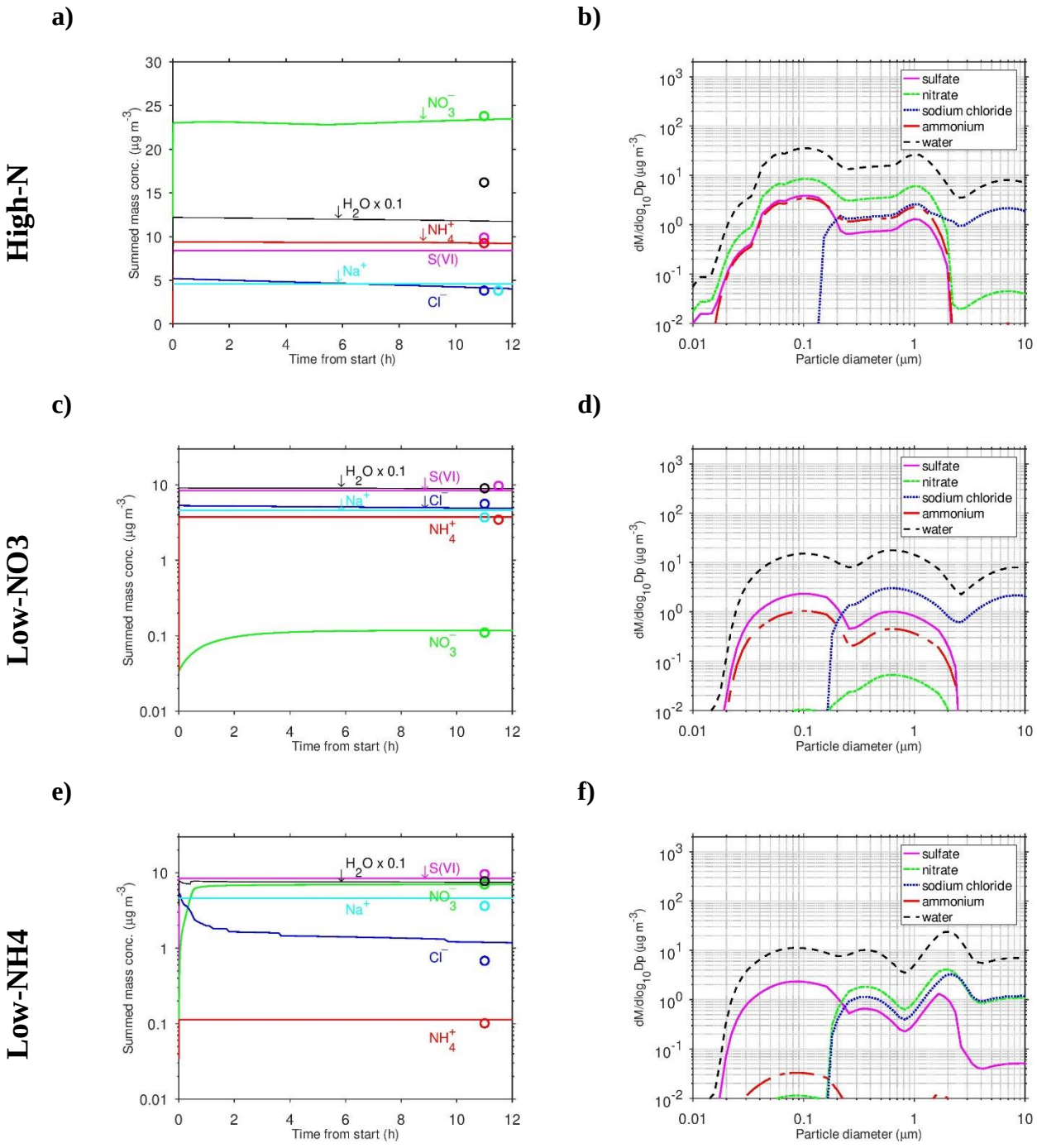

Figure S2. Results from Case 3. Parts a, c, e: summed particle mass concentrations, circles represent the solution from an equilibrium calculation with EQUISOLV II adopted from Jacobson (2005a). Note the logarithmic scale of the vertical axis in parts c) and e); parts b, d, f: final mass size distributions after 12 h simulation time; component mass distributions were constructed from total mass distribution and modal mass fractions. Sodium chloride is the sum of Na^+ and Cl^-.

The test with extremely low ammonia is considered to be most vulnerable towards oscillations at long operator time-split interval and the solution might become unstable (Jacobson, 2005a). The simulated time-series of summed mass concentrations from MAFOR were smooth, showing no sign of oscillation (Fig. S2c). The accuracy is as high as for the simulation with PNG-EQUISOLV II using an operator-split time interval of 5 s (Jacobson, 2005a; figure 4 therein). The equilibrium in "Low-NH4" was reached after ca. 5 h simulation time for all dissolved/dissociated species.

Fig. S2f shows substantial formation of both nitrate and sulfate in the coarse mode in "Low-NH4". In sea-salt (here represented as sodium chloride, NaCl) aerosol under acidic conditions, HNO_3 displaces the Cl^- ion in a heterogeneous reaction that forms $NaNO_3$ and gas-phase HCl, resulting in aerosol chloride depletion (Brimblecombe and Clegg, 1988). The loss of chloride occurred relatively fast, with a 63 % reduction after 1 h, similar as in the corresponding case (76 % reduction after 1h) with high acid concentration and RH = 90 % presented in Jacobson (2005a). Simulated chloride from the PNG-MOSAIC scheme was not reduced as much as in the equilibrium solution from EQUISOLV II, which is attributable to differences in the reaction rate constant used in MOSAIC for the irreversible heterogeneous reaction of gaseous HNO_3 with solid/aqueous phase NaCl. In MOSAIC, this reaction is assumed to proceed to completion until all solid NaCl is exhausted (Zaveri et al., 2008). MOSAIC also considers chloride depletion with sulphuric acid.

References

Anand, S., Mayya, Y. S., Yu, M., Seipenbusch, M., and Kasper, G.: A numerical study of coagulation of nanoparticle aerosols injected continuously into a large, well stirred chamber, J. Aerosol Sci., 52, 18–32, doi:10.1016/j.jaerosci.2012.04.010, 2012.

Binkowski, F. S. and Shankar, U.: The regional particulate matter model. 1: Model description and preliminary results, J. Geophys. Res., 100, 26,191–26,209, 1995.

Brimblecombe, P. and Clegg, S.: The solubility and behavior of acidic gases in the marine aerosol, J. Atmos. Chem., 7, 1–18, doi:10.1007/BF00048251, 1988.

Hussein, T., Kukkonen, J., Korhonen, H., Pohjola, M., Pirjola, L., Wraith, D., Härkönen, J., Teinilä, K., Koponen, I. K., Karppinen, A., Hillamo, R., and Kulmala, M.: Evaluation and modeling of the size fractionated aerosol particle number concentration measurements nearby a major road in Helsinki – Part II: Aerosol measurements within the SAPPHIRE project, Atmos. Chem. Phys., 7, 4081–4094, doi:10.5194/acp-7-4081-2007, 2007.

Jacobson, M. Z.: A solution to the problem of nonequilibrium acid/base gas-particle transfer at long time step, Aerosol Sci. Technol., 39(2), 92–103, doi:10.1080/027868290904546, 2005a.

Korhonen, H., Lehtinen, K. E. J., Pirjola, L., Napari, I., Vehkamäki, H., Noppel, M., and Kulmala M.: Simulation of atmospheric nucleation mode: A comparison of nucleation models and size distribution descriptions, J. Geophys. Res., 108, D15, 4471, doi:10.1029/2002JD003305, 2003.

Määttänen, A., Merikanto, J., Henschel, H., Duplissy, J., Makkonen, R., Ortega, I. K., and Vehkamäki, H.: New parameterizations for neutral and ion-induced sulfuric acid-water particle formation in nucleation and kinetic regimes, J. Geophys. Res. Atmospheres, 123, 1269-1296. https://doi.org/10.1002/2017JD027429, 2018a.

Pohjola, M. A., Pirjola, L., Kukkonen, J., and Kulmala, M.: Modelling of the influence of aerosol processes for the dispersion of vehicular exhaust plumes in street environment, Atmos. Environ., 37, 339–351, 2003.

A. Prakash, A., Bapat, A. P., and Zachariah, M. R.: A simple numerical algorithm and software for solution of nucleation, surface growth, and coagulation problems, Aerosol Sci. Technol., 37(11), 892–898, doi:10.1080/02786820300933, 2003.

Seipenbusch, M., Binder, A., and Kasper, G.: Temporal evolution of nanoparticle aerosols in workplace exposure, Ann. Occup. Hyg., 52(8), 707–716, doi:10.1093/annhyg/men067, 2008.

Zaveri, R. A., Easter, R. C., Fast, J. D., and Peters, L. K.: Model for Simulating Aerosol Interaction and Chemistry (MOSAIC), J. Geophys. Res., 113, D13204, doi:10.1029/2007JD008782, 2008.